Progress In Electromagnetics Research M, Vol. 31, 13–27, 2013

A LOOP-TYPE END-LAUNCHER FOR CARBON FIBER REINFORCED POLYMER WAVEGUIDES

Alexe Bojovschi[1, *], Derek Gray[2], and Kamran Ghorbani[1]

[1]Electrical and Computer Engineering, RMIT University, Melbourne, VIC 3001, Australia

[2]Department of Electrical and Electronic Engineering, University of Nottingham, Ningbo 315100, China

Abstract—The analysis of an end-launcher type transition from coaxial to WR90 waveguides is presented. This transition is tuned to have the highest performance at the radar frequency of 9.375 GHz. The characteristics of the transducer are investigated comparatively in 30 cm aluminum and carbon fiber reinforced polymer waveguides. The advantage of the proposed feed is that it does not require grounding to the broad wall of the waveguide compared to the traditional end-launcher loop feeds. This departure from the current loop feeds makes the proposed feed suitable for carbon fiber reinforced polymer waveguides where a disruption in the broad wall would be undesirable.

1. INTRODUCTION

Various collinear end-on transitions, implemented in waveguides over different frequency bands, have been proposed. These transitions create the family of microwave components that find wide applications in microwave and waveguide techniques. Among these the most popular and well investigated are the loop transitions [1–3] and the stepped or linearly tapered ridge waveguide sections [4, 5]. In these launchers the grounding is achieved by direct connection to the broad wall. Posts that slide through slots in the broad wall are also used for adjusting the impedance of the waveguide section of interest to improve matching [5]. Wheeler reported the first loop transition in 1957 [6]. Later on the loop type end feed was adapted for a multimode phase array element [7]. Although these feeds were available, Das and Sanyal prepossessed design formulas in 1976 for a concentric loop [8].

Received 16 April 2013, Accepted 10 May 2013, Scheduled 19 May 2013

* Corresponding author: Alexe Bojovschi (alexe.bojovschi@rmit.edu.au).

In their work the dimensions of the L shaped loop were chosen so that the real part of the input impedance seen by the coaxial line was equal to the characteristic impedance of the coaxial line. The input reactance cancelation was obtained by a trial and error method. The same authors together with Deshpande reported an improved formulation that takes into account the explicit expression of both real and imaginary parts of the input impedance seen by coaxial line in terms of loop dimensions [2]. The centric as well as offset loop feeds, were implemented in circular and rectangular waveguides [2, 3].

The end-launcher type feeds are the appropriate choice for increased compactness of waveguide phase array antennas. The integration of antennas in the structure of an avionics system element such as the wings or the fuselage has the potential to reduce the weight and the cost of airplanes, in the same time providing both electromagnetic and structural functions. This technology, which aims to increase the performance of air vehicles by overcoming the limitations of traditional antennas, which increase aerodynamic drag, is termed CLAS (Conformal Load-bearing Antenna Structure) [9, 10]. One potential implementation of CLAS for Ground Moving Target Indicator (GMTI)/Synthetic Aperture Radar (SAR) radar is Slotted Waveguide Antenna Stiffened Structure (SWASS) [11]. In SWASS the top-hat stiffeners on thin skins or blade stiffeners in sandwich skins both support structural load and act as radiofrequency waveguides [10, 12]. Slots cut through the outer skin and into the waveguides produce slotted waveguide antenna arrays [13]. The slots are filled with dielectric to restore the exterior surface. SWASS may be manufactured from any structural material however in aircraft applications this is most likely to be carbon fibre reinforced polymer (CFRP). The high specific stiffness and strength, and low susceptibility to corrosion and fatigue cracking [14, 15], of this material make it suitable for weight critical aeronautical application.

Due to its exceptional mechanical and suitable RF properties CFRP has been used recently for many microwave applications. These include waveguides [16, 17] where the goal is to develop slotted waveguide antenna array systems made of CFRP. A frequency selective polarizing subrefector manufactured from unidirectional CFRP was reported [18]. The work shows that the reflector can reduce the cross polarization by about 13 dB at S-band and the incident angle has minimum consequence on the frequency response of the polarizer. The use of CFRP for microstrip patch, slot antenna and capacitively fed cavity-backed slot antenna has also been considered [19–21]. The studies show the advantage of backing the slots with a CFRP cavity leads to an enhancement in gain by 2 dB and of front-to-back-ratio by

13 dB.

The presence of defects such as cavities in dielectric materials such as epoxy resin is known to lead to partial discharge and ultimately to the breakdown of the dielectric insulator [22]. This is applicable also to CFRP composites where the carbon fibres are encapsulated in an epoxy matrix. Methods to detect defects in CFRP have also been developed [23] to prevent imminent failures of these composites when used in critical applications such as on a fuselage of an airplane. The dimensional stability of CFRP for space antenna missions was explored [24]. As the material for these applications not only should be strong, stiff and light but also have to provide dimensional stability. CFRP is shown to be one of the most promising candidates for these missions.

In this work we report a loop type end-launcher optimized for a CFRP planar array panel with 9.375 GHz radiating slots. The requirements of keeping the integrity of the CFRP waveguide walls intact led to a loop feed that does not require grounding to the broad wall. This is of relevance as a discontinuity in the broad wall reduces the structural integrity of the waveguide component. The proposed feed is investigated in CFRP waveguide using computational and experimental methods. The characteristics of CFRP layers, of the waveguide walls, with the fibre orientation [90 0 0 90] = $[90, 0]_s$, which impact directly on the reflection and transmission coefficients, are accounted for using an experimentally validated electromagnetic anisotropic model [16]. The results are compared with those in an aluminum waveguide.

2. METHOD

2.1. Computational Method

Finite Element Method (FEM) as implemented in Ansoft's High Frequency Structure Simulator (HFSS) [25] computational electromagnetic software was used. FEM was established in 1942 when Courant used piece wise linear approximations on a set of triangles, which he called "elements" [26]. The method was first applied in electromagnetics during the 1960s [27]. In this work FEM relies on an integral formulation of the variational boundary value problem [27]. In this method the volume of interest is subdivided in surface or volume elements where the unknown function is approximated as a polynomial. An adaptive meshing is used in the calculations. In this manner the finite element mesh is created and automatically refined in the areas of highest error. This allows increasing the accuracy of the succeeding adaptive solution.

In HFSS the wave ports are connected to uniform waveguides with the same cross-section as the ports. The power at port 1 (Figure 1) is the time-averaged power P. The power is calculated using Equation (1),

$$P = \Re \int_A E \times H^* \cdot dS \tag{1}$$

where $\Re$ is the real part of a complex number or function, A is the surface area, $\mathbf{E}$ is the tensor of the electric field, $\mathbf{H}^*$ is the conjugate tensor of the magnetic field and dS is the unit surface area.

A waveguide supports an infinite number of modes. The electric field for the ports specified can be written as:

$$\mathbf{E}_m(x, y, z, t) = \Re \left[\mathbf{E}_m(x, y) e^{j\omega t - \gamma_m z} \right] \tag{2}$$

where $\mathbf{E}_m(x, y)$ is the electric field mode pattern of mode m, $\gamma_m = \alpha_m + \beta_m$ the complex propagation constant of mode m where α_m is the attenuation constant of mode m and β_m the propagation constant of mode m that determines how the phase angle varies with z at a specific time t, $\omega = 2\pi f$ the angular frequency of oscillation, and j the imaginary unit equal with $\sqrt{-1}$. In this case, x and y-axes are situated in the cross-section of the port, and the z-axis corresponds to the direction of propagation.

The field pattern inside the waveguide can be determined by solving Maxwell equations. The wave port solver used computes, for each mode m specified, the electric field mode pattern $\mathbf{E}_m(x, y)$ and the propagation constant γ_m using Equation (2).

$$\nabla \times \left(\frac{1}{\mu_r} \nabla \times \mathbf{E}_m(x, y) e^{-\gamma_m z} \right) - k_0^2 \varepsilon_r \mathbf{E}_m(x, y) e^{-\gamma_m z} = 0 \tag{3}$$

In this equation $k_0 = \omega/c$ is the wave number of the free space, $\mu_r(x, y, z)$ the complex relative permeability, and $\varepsilon_r(x, y, z)$ the complex anisotropic relative permittivity tensor. The port solver also solves $H_m(x, y)$ by using a corresponding equation for the magnetic field. It can be noted from Equation (2) that the excitation field pattern obtained is valid only at a specific frequency. For different frequencies of interest in the X-band different excitation field patterns are computed.

The intensity of the field over the radiation surface is used to calculate the field surrounding the waveguides. This is relevant for carbon fibre waveguides, where the fields leak out through the walls, but irrelevant for aluminium or cupper waveguides. The space surrounding the waveguides is divided in two domains: near-field region

and far-field region. The electric field $\mathbf{E}(x, y, z)$ external to a region bounded by a close surface may be written as:

$$\mathbf{E}(x, y, z) = \int_s \left(\langle j\omega\mu_0 H_{\tan}\rangle G + \langle E_{\tan} \times \nabla G\rangle + \langle \mathbf{E}_{normal} \nabla G\rangle\right) ds \quad (4)$$

where s is the radiation boundary surface, μ_0 the relative permeability of the free space, $\mathbf{H}_{\tan}$ the component of the magnetic field tangential to the surface, $\mathbf{E}_{normal}$ the component of the electric field that is normal to the surface, $\mathbf{E}_{\tan}$ the component of the electric field tangential to the surface, and $G = (e^{-jk_0|\mathbf{r}-\mathbf{r}_0|\sqrt{\mu_r\varepsilon_r}})/|\mathbf{r}-\mathbf{r}_0|$ the Green's function in free space. In this function $k_0 = \omega\sqrt{\mu_0\varepsilon_0}$ is the free space wave number, $\mathbf{r}$ the filed points, $\mathbf{r}_0$ the source points on the integrated surface, $\varepsilon_0 = 1/c^2\mu_0$ the permittivity of the free space, ε_r the relative anisotropic permittivity of CFRP, and μ_r its relative permeability.

Models of waveguide feeds and CFRP waveguides were developed. The ply stacking sequence for the CFRP waveguides used in this work is $[90,\ 0]_s$, where the 0° fibre direction is parallel to the waveguide longitudinal axis. A recently developed and validated model of the electrical anisotropy of CFRP was reported [16]. This model is applied to the CFRP waveguide walls in order to provide accurate electromagnetic characterization. This involve defining the electrical anisotropy of CFRP via the relative complex permittivity and the effective conductivity tensors:

$$\varepsilon_0^a = \begin{bmatrix} \varepsilon_0^x & 0 & 0 \\ 0 & \varepsilon_0^y & 0 \\ 0 & 0 & 0 \end{bmatrix} \quad (5)$$

$$\sigma_0^a = \begin{bmatrix} 0 & 0 & 0 \\ 0 & 0 & 0 \\ 0 & 0 & \sigma_0^z \end{bmatrix} \quad (6)$$

$$\varepsilon_{90}^a = \begin{bmatrix} 0 & 0 & 0 \\ 0 & \varepsilon_{90}^y & 0 \\ 0 & 0 & \varepsilon_{90}^z \end{bmatrix} \quad (7)$$

$$\sigma_{90}^a = \begin{bmatrix} \sigma_{90}^x & 0 & 0 \\ 0 & 0 & 0 \\ 0 & 0 & 0 \end{bmatrix} \quad (8)$$

$$\varepsilon_0^b = \begin{bmatrix} \varepsilon_0^x & 0 & 0 \\ 0 & \varepsilon_0^y & 0 \\ 0 & 0 & 0 \end{bmatrix} \quad (9)$$

$$\sigma_0^b = \begin{bmatrix} 0 & 0 & 0 \\ 0 & 0 & 0 \\ 0 & 0 & \sigma_0^z \end{bmatrix} \tag{10}$$

$$\varepsilon_{90}^b = \begin{bmatrix} \varepsilon_{90}^x & 0 & 0 \\ 0 & 0 & 0 \\ 0 & 0 & \varepsilon_{90}^z \end{bmatrix} \tag{11}$$

$$\sigma_{90}^b = \begin{bmatrix} 0 & 0 & 0 \\ 0 & \sigma_{90}^x & 0 \\ 0 & 0 & 0 \end{bmatrix} \tag{12}$$

where a and b indicate the broad and respectively the narrow wall of the waveguide. The values of the components of the anisotropic permittivity tensor are [16]:

$$\varepsilon_0^x = \varepsilon_0^y = \varepsilon_0^z = 30 - j7.4 \tag{13}$$

$$\varepsilon_{90}^x = \varepsilon_{90}^y = \varepsilon_{90}^z = 30 - j7.4 \tag{14}$$

The effective anisotropic conductivity of the CFRP laminate was obtained from experimental waveguide attenuation measurements over the entire X-band [16]. For example at 10 GHz the conductivity components are well approximated by:

$$\sigma_0^z = \sigma_{90}^x = \sigma_{90}^y = 28 \times 10^4 \,\mathrm{S/m} \tag{15}$$

A well designed waveguide feed will induce minimal power loss when it transforms the transverse electromagnetic (TEM) mode in the coaxial feed line to the transverse electric (TE) mode in the waveguide [3]. The model of the proposed end-launcher feed is shown in Figure 1. The xy coordinates of the centre conductor of the SubMiniature version A (SMA) connector correspond to the xy coordinates of the centre of the waveguide cross-section. The dimensions of the feed presented in Figure 1 are as follows: $l = 16.00\,\mathrm{mm}$, $h = 5.08\,\mathrm{mm}$, $w = 3.00\,\mathrm{mm}$ and $t = 0.13\,\mathrm{mm}$. The feed consists of four sections (s_1, s_2, s_3 and s_4) and is grounded to the SMA connector through section s_4. For a small thickness (t) of *section* s_3 one can approximate the equivalent circuit for this type of loop feed with the one where grounding is obtained by directly connecting section s_2 to the broad wall [3]. The equivalent circuit includes input impedance seen by the coaxial line described by the stationary formula [28]:

$$Z_{in} = -\frac{1}{I_{in}^2} \int\limits_v E_{s_1 s_2} \cdot J_{s_1 s_2} dV \tag{16}$$

where I_{in} is the total input current and $E_{s_1 s_2}$ the electric field due to the current density ($J_{s_1 s_2}$) on sections p, s_1 and s_2. A capacitive component would describe the gap between the loop sections and

waveguide walls. This includes the capacitance between section s_1 and the waveguide walls and a capacitance, present only in experiments, between section s_3 and bottom wall of the waveguide. By considering the interaction between the current in the section p and s_1 and the electric field excited by the full length of the loop feed the reactive component, associated with higher order modes, can be derived for this section [3]. In the same manner the resistive component and reactive component, due to the interaction between the current density in section s_2 and electric field excited by the entire loop feed, can be derived [3].

The waveguide walls consist of either CFRP or aluminium alloy. The CFRP waveguide walls are made of four plies of aerospace grade IM7/977-3 CFRP prepreg tape [29] with a ply stacking sequence of $[90\ 0]_s$. The thickness of each ply is 125 µm giving a total wall thickness of $c = 0.50$ mm. The effective conductivity of this material at 9.375 GHz parallel to the fibres is 28.98×10^3 S/m [16]. Transverse to the fibres (both in-plane and out-of-plane) it acts as a lossy dielectric with complex permittivity of $30 - 7.4j$ [16]. The electrical anisotropic model used includes also the frequency dependence of CFRP conductivity over X-band [16]. The conductivity of aluminium is 36×10^6 S/m. A 30 mm layer of air and a further 50 mm of Perfectly Matched Layer (PML) surrounded the end-launch waveguide system in all simulations.

The end-launcher was fed through a wave port (Port 1) placed on the cross-section of the inner conductor of a standard SMA connector (Figure 1). A second port (Port 2) with the size equal with the inner cross-section of the waveguide, located at the far end of the waveguide

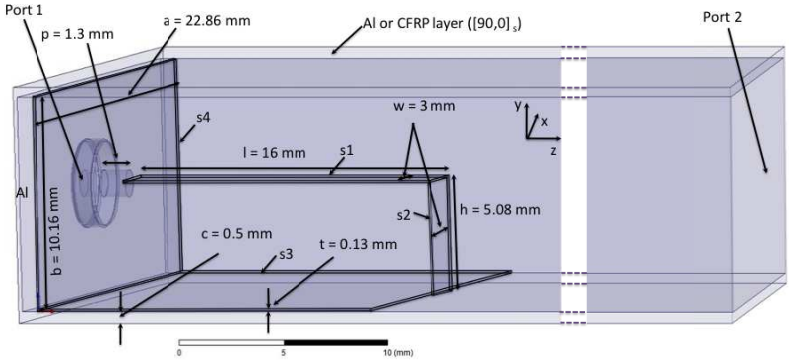

Figure 1. Schematic representation of the end-launch RF feed, consisting of a 16 mm long ×5.08 mm high ×3 mm wide loop in a WR90 waveguide.

was included to allow for the transmission coefficient to be calculated. The radius of the SMA inner conductor is 0.325 mm and that of the outer conductor is 2.10 mm. The permittivity of the dielectric materials that separated the two conductors of the SMA is 2.08. The SMA inner conductor protruded by $p = 1.3$ mm into the waveguide, where it is connected electrically to section s_1.

The reflection coefficients were calculated for different end-launcher dimensions. The error tolerance of the sweep calculations was set to 0.5% and a maximum of 250 solutions were considered for the interpolation sweep. The dimensions of the end-launcher were optimized to produce minimal reflection coefficient ($|s_{11}|$) at 9.375 GHz.

2.2. Experimental Method

Three hundred mm long sections of CFRP and aluminium waveguide plus the optimal feed, as shown in Figure 2, were manufactured. The process for manufacturing the waveguides from aerospace grade Cytec IM7/977-3 prepreg tape has been detailed elsewhere [16, 30]. The proposed end-launchers were manufactured from a single piece of $t = 0.13$ mm thick brass shim. The narrow end of the loop was soldered to the pin of the SMA connector while the wide end was soldered to the outer conductor of the SMA. The loops were supported by aluminum blocks machined for a close sliding fit within the waveguide. The aluminium block has two section of high impedance measuring 20.7 mm × 22.83 mm × 10.12 mm and 10.1 mm × 22.83 mm × 10.12 mm and a cylindrical section of low impedance measuring 10.1 mm in length with a radius of 3.58 mm. This design is required to prevent higher order modes [31, 32] when the loop feed is inserted in a standing wave slotted waveguide antenna. A Wiltron 360B vector network

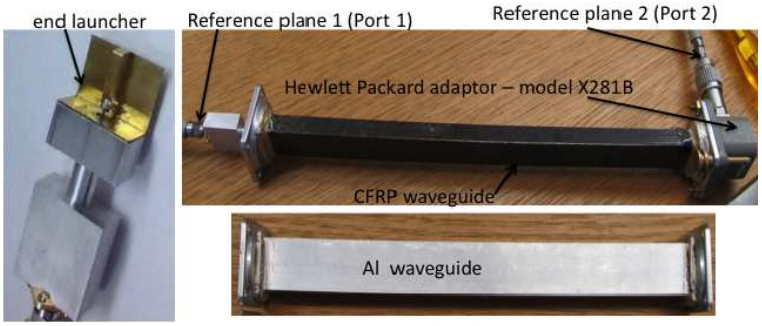

Figure 2. Al and CFRP waveguides and the slide in loop end launcher.

analyzer was used to measure the reflection ($|s_{11}|$) and transmission ($|s_{21}|$) coefficients. A 12-term Thru-Reflect-Line (TRL) calibration method [33] was used and 200 points were utilized for averaging. An Anritsu SMA/3.5 mm calibration kit, model 3650, was employed. The use of the Hewlett Packard waveguide adaptor (Figure 2) introduces a very small extra loss in the transmission line, of orders of 0.01 dB over the frequency band, which has been ignored in this study.

3. RESULTS AND DISCUSSIONS

The following three steps were used in the numerical modelling to design the optimal end-launcher dimensions (i) a parametric analysis of the feed dimensions, (ii) an optimization process and (iii) a sensitivity assessment of the feed parameters to manufacturing tolerances. The simulated effect of pin length (p) on reflection coefficient is shown in Figure 3. Minimum reflection coefficient at 9.375 GHz is predicted to require a pin length of $p = 1.3$ mm. Similarly, as shown in Figure 4, the resonant frequency could be controlled by varying the loop length (l).

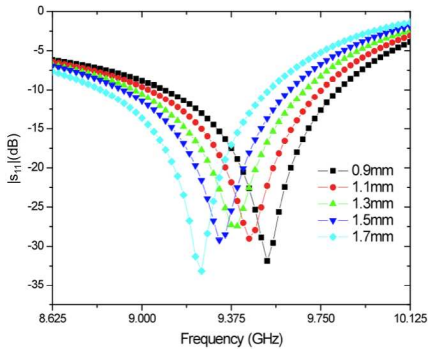

Figure 3. Illustrative values of the return loss during pin length (p) optimization.

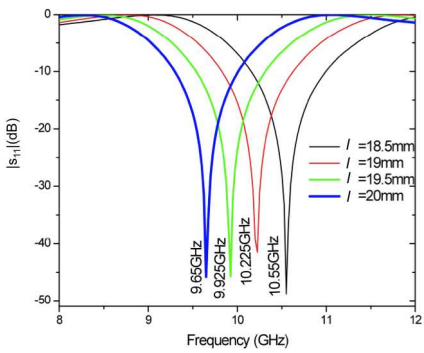

Figure 4. Tuning the length (l) of the loop feed for the required frequency.

A sensitivity study is conducted in order to evaluate the effect of finite manufacturing tolerances on the loop feed. Figure 5 shows the mean and standard deviation of the return loss when the optimal dimensions shown in Figure 1 are varied in the following way: $l = 16.00$ mm varied from 15.17 to 16.64 mm in steps of 0.20 mm, $p = 1.30$ mm varied from 1.20 to 1.40 mm in steps of 0.02 mm, $t = 0.130$ mm varied from 0.115 to 0.145 mm in steps of 0.005 mm and $w = 3.00$ mm

varied from 2.90 to 3.10 mm in steps of 0.02 mm. Figure 5 indicates that the reflection coefficient remained below −10 dB despite the dimensional variations.

The predicted and measured $|s_{11}|$ and $|s_{21}|$ for the optimised feed in the CFRP and aluminium waveguides are presented in Figure 6. The transmission coefficients at 9.375 GHz were 0.06 dB for the aluminium waveguide and 1.77 dB for the CFRP waveguide. The high loss in the CFRP system is attributed exclusively to losses in the CFRP waveguide itself, and not due to the feed. Previous work showed that the attenuation loss over a 300 mm length of CFRP waveguide would be approximately 1.7 dB [16]. The reflection coefficients curves in Figure 6 showed reasonable agreement between predicted and measured coefficients, with resonance at 9.375 GHz for all cases. Differences in the depth of the trough were attributed to the effect of manufacturing tolerance. As predicted (Figure 5), tens of micrometer variation in the dimensions of the feed could change the reflection coefficient at resonance by up to 30 dB.

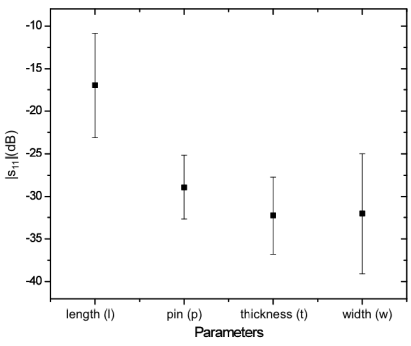

Figure 5. Expected sensitivity of end-launcher parameters to manufacturing process.

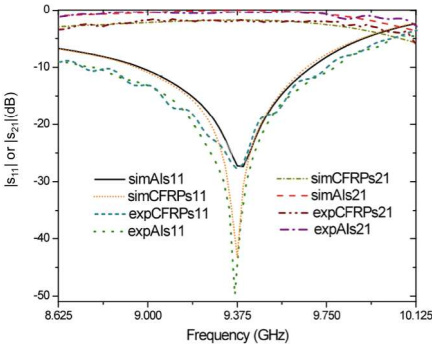

Figure 6. Reflection and transmission parameter for the loop feed from simulation (sim) and experimental (exp) investigations in aluminium and CFRP waveguides.

The surface current density, induced by classical and the proposed end launcher, on the broad wall of the aluminium and CFRP waveguides and on section s_3 (Figure 1) is assessed (Figure 7). It should be noted that section p, s_1 and s_2 are the same for both end launchers. The results indicate low current injection in the broad wall by the loop proposed in this work. This is desirable to be maintained at a minimum when relatively high power is fed into the launcher. In CFRP waveguides the approximately 0.3 µm epoxy layer, that

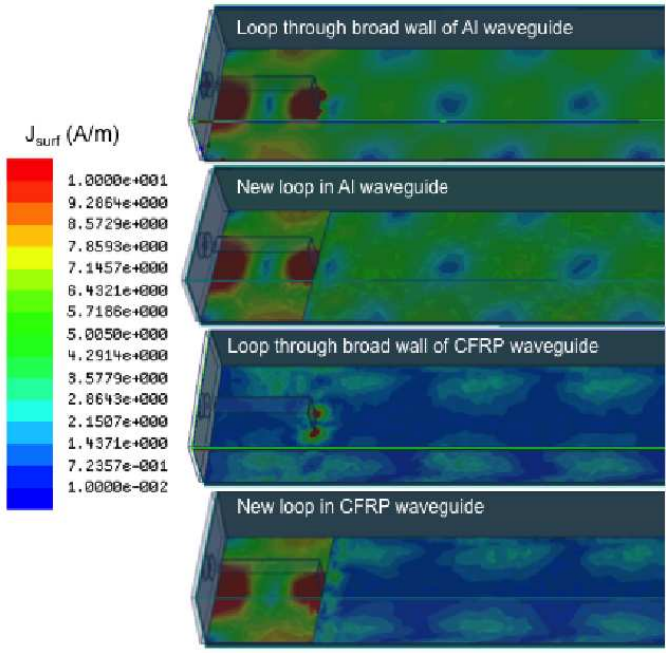

Figure 7. Current density distribution on the bottom broad wall in CFRP and Al waveguide for 0 phase of the source and 9.375 GHz.

encapsulates the carbon fibres, can deteriorate under sustained high temperature induced by high current densities. This in turn can lead to fibre exposure, which in contact with oxygen can undergo galvanic corrosion. The illustrative surface currents in Figure 7 for 4 different systems correspond to a frequency of 9.375 GHz when the feeds are excited with a 0° phase TEM mode. The figure indicates that there is a higher current density concentration at the grounding point for a classical loop end launcher. For this case the energy is dissipated in the broad wall. For the proposed feed it can be noticed that the current density is distributed mainly in the s_3 section of the loop.

Quantitative results of the maximum value of surface current density on the broad wall are presented in Figure 8 together with the values of reflection and transmission coefficients for the investigated systems. The plot shows significant difference in the current density on the bottom broad wall for both aluminium and CFRP waveguides when excited by the classical loop feed and the proposed launcher. It can be noticed that the maximum current density for the classical feed in the CFRP waveguide is 92.016 A/m while for the proposed launcher

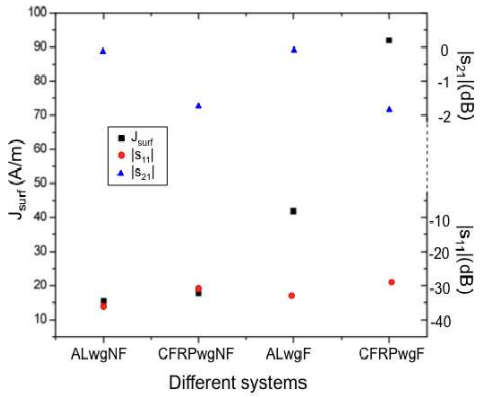

Figure 8. Maximum value of the surface current density on the broad wall of the WR90 aluminium (AL) and CFRP waveguides (wg) with classical loop feed (F) and the proposes loop feed (NF). The reflection and transmission coefficients for these systems are also presented.

is 17.84 A/m. From Figure 8, it can be observed also an improvement in the reflection and transmission coefficients. The value of $|s_{21}|$ at 9.375 GHz for the proposed launcher is 1.772 dB while for the classic feed is 1.898 dB. In this work a source with a power of 1 W excited the loops. A study that will assess the temperature profile in the broad wall as a function of input power would be of interest.

4. CONCLUSION

A loop-type end-launcher feed was developed to transition from coaxial to WR90 waveguides manufactured from CFRP. The key feature of this feed is that it does not require a "hard" electrical connection with the carbon fibres. This characteristic of the end launcher leads also to a significant decrease of the current injected in the broad wall. The feed, optimised for 9.375 GHz, was manufactured and tested in waveguides manufactured from aluminium and aerospace grade IM7/977-3 CFRP. The proposed feed can be used in lightweight microwave applications such as in a planar slotted waveguide antenna array made of CFRP.

ACKNOWLEDGMENT

The authors thank Associate Professor Wayne Rowe for constructive discussions. The work conducted for this report was funded anonymously.

REFERENCES

1. Chan, K. K., R. Martin, and K. Chadwick, "A broadband end launcher coaxial-to-waveguide transition for waveguide phased arrays," *Proceedings of IEEE*, 1390–1393, 1998.
2. Deshpande, M. D., B. N. Das, and G. S. Sanyal, "Analysis of an end launcher for an X-band rectangular waveguide," *IEEE Transactions on Microwave Theory and Techniques*, Vol. 27, No. 8, 731–735, Aug. 1979.
3. Saad, S. M., "A more accurate analysis and design of coaxial-to-rectangular waveguide end launcher," *IEEE Transactions on Microwave Theory and Techniques*, Vol. 38, No. 2, 129–134, Feb. 1990.
4. Levy, R. and L. W. Hendrick, "Analysis and synthesis of in-line coaxial-to-waveguide adapters," *Proceedings of IEEE Microwave Symposium,* 809–811, Seattle, USA, Jun. 2002.
5. Dix, J. C., "Design of waveguide/coaxial transition for the band 2.5–4.1 Gc/s," *Proc. of the Institute of Electrical Engineers*, Vol. 110, No. 2, 253–255, Feb. 1963.
6. Wheeler, G. J., "Broad band waveguide to coaxial transitions," IRE Convention Record Part 1, 182–185, 1957.
7. Tang, R. and N. S. Wong, "Multimode phased array element for wide scan angle impedance matching," *Proceedings of IEEE*, 1951–1959, 1968.
8. Das, B. N. and G. S. Sanyal, "Coaxial to waveguide transition (end launcher type)," *Proc. of the Institute of Electrical Engineers*, Vol. 110, 253–255, London, 1963.
9. Lockyer, A. J., K. H. Alt, D. P. Coughlin, M. D. Durham, J. N. Kudva, A. C. Goetz, and J. Tuss, "Design and development of a conformal load-bearing smart skin antenna: Overview of the AFRL smart skin structures technology demonstration (S^3TD)," *Proc. of SPIE*, Vol. 3674, 4010–4024, 1999.
10. Callus, P. J., "Novel concepts for conformal load-bearing antenna structure," Report No. DSTO-TR-2096, Defence Science and Technology Organisation, Australia, Feb. 2008.
11. Callus, P. J., J. C. D. de LaHarpe, J. M. Tuss, W. G. Baron, and D. G. Kuhl, "Slotted waveguide antenna stiffened structure," United States Patent No. 8149177, Apr. 3, 2012.
12. Nicholson, K. J. and P. J. Callus, "Antenna patterns from single slots in carbon fibre reinforced plastic waveguides," Report No. DSTO-TR-2389, Defence Science and Technology Organisation, Australia, Feb. 2010.

13. Stevenson, A. F., "Theory of slots in rectangular waveguides," *J. Appl. Phys.*, Vol. 19, 24–38, 1948.
14. Golfman, Y., *Hybrid Anisotropic Materials for Structural Aviation Parts,* Taylor & Francis Group, 2011.
15. Niu, M. C. Y., *Composite Airframe Structures,* 2nd Edition, Conmilit Press Ltd., Hong Kong, 1996.
16. Bojovschi, A., K. J. Nicholson, A. Galehdar, P. J. Callus, and K. Ghorbani, "The role of fibre orientation on the electromagnetic performance of waveguides manufactured from carbon fibre reinforced plastic," *Progress In Electromagnetics Research B*, Vol. 39, 267–280, 2012.
17. Gray, D., K. J. Nicholson, K. Ghorbani, and P. J. Callus, "Carbon fibre reinforced plastic slotted waveguide antenna," *Proc. Asia Pacific Microwave Conf.*, 307–310, 2010.
18. Galehdar, A., W. S. T. Rowe, K. Ghorbani, P. J. Callus, S. John, and C. H. Wang, "A frequency selective polarizer using carbon fibre reinforced polymer composite," *Progress In Electromagnetics Research C*, Vol. 25, 107–118, 2012.
19. Galehdar, A., W. S. T. Rowe, K. Ghorbani, P. J. Callus, S. John, and C. H. Wang, "The effect of ply orientation on the performance of antennas in or on carbon fibre composites," *Progress In Electromagnetics Research*, Vol. 116, 123–136, 2011.
20. Mehdipour, A., A.-R. Sebak, C. W. Trueman, I. D. Rosca, and S. V. Hoa, "Performance of microstrip patch antenna on a reinforced carbon fiber composite ground plane," *Microwave and Optical Technology Letters*, Vol. 53, No. 6, 1328–1331, 2011.
21. Galehdar, A., P. J. Callus, W. S. T. Rowe, C. H. Wang, S. John, and K. Ghorbani, "Capacitively fed cavity-backed slot antenna in carbon-fiber composite panels," *IEEE Antenna and Wireless Propagation Letters*, Vol. 11, 1028–1031, 2012.
22. Bojovschi, A., W. R. Rowe, and K. L. Wong, "Electromagnetic field intensity generated by partial discharge in high voltage insulating materials," *Progress In Electromagnetics Research*, Vol. 104, 167–182, 2010.
23. Megali, G., D. Pellicano, M. Cacciola, S. Calcagno, M. Versaci, and F. C. Morabito, "EC modeling and enhancement signals in CFRP inspection," *Progress In Electromagnetics Research M*, Vol. 14, 45–60, 2010.
24. Sanjuán, J., A. Preston, D. Korytov, A. Spector, A. Freise, G. Dixon, J. Livas, and G. Mueller, "Carbon fiber reinforced polymer dimensional stability investigations for use on the

laser interferometer space antenna mission telescope," *Review of Scientific Instruments*, Vol. 82, 124501-1–124501-11, 2011.

25. Ansoft HFSS 12.1.2, Online Resource, 2010.
26. Silvester, P. P. and G. Pelosi, *Finite Elements for Wave Electromagnetics,* IEEE Press, New York, 1996.
27. Davidson, D. B., *Computational Electromagnetics for RF for Microwave Engineering,* Cambridge University Press, Cambridge, 2005.
28. Harington, R. F., *Time Harmonic Electromagnetic Fields,* Section 8.11, McGraw-Hill, New York, 1961.
29. Hexcel Corporation, HexTow IM7 Carbon Fibre Product Data Sheet.
30. Callus, P. J. and K. J. Nicholson, "Standard operating procedure — Manufacture of carbon fibre reinforced plastic waveguides and slotted waveguide antennas," Report No. DSTO-TN-0937, Version 1.0, Defence Science and Technology Organisation, Australia, Jun. 2011.
31. Brewer, M. K. and A. V. Räisänen, "Dual-harmonic noncontacting millimeter waveguide backshorts: Theory, design, and test," *IEEE Transactions on Microwave Theory and Techniques*, Vol. 30, 708–714, 1982.
32. McGrath, W. R., T. M. Weller, and L. P. B. Katehi, "Novel noncontacting waveguide backshort for submilimeter wave frequencies," *Int. J. of Infrared and Millimeter Waves*, Vol. 16, No. 1, 237–256, 1995.
33. Wiltron 360, "Vector network analyser operation manual," Wiltron, Morgan Hill, CA, 1994.